

Forward THz radiation emission by femtosecond filamentation in gases: theory and experiment

Ciro d'Amico, Aurélien Houard, Selcuk Akturk, Yi Liu, J. Le Bloas, Michel A. Franco, Bernard Prade, Arnaud Couairon, Vladimir Tikhonchuk, André Mysyrowicz

▶ **To cite this version:**

Ciro d'Amico, Aurélien Houard, Selcuk Akturk, Yi Liu, J. Le Bloas, et al.. Forward THz radiation emission by femtosecond filamentation in gases: theory and experiment. New Journal of Physics, 2008, 10, pp.013015. 10.1088/1367-2630/10/1/013015 . hal-00454582

HAL Id: hal-00454582

https://polytechnique.hal.science/hal-00454582

Submitted on 8 Feb 2010

HAL is a multi-disciplinary open access archive for the deposit and dissemination of scientific research documents, whether they are published or not. The documents may come from teaching and research institutions in France or abroad, or from public or private research centers.

L'archive ouverte pluridisciplinaire **HAL**, est destinée au dépôt et à la diffusion de documents scientifiques de niveau recherche, publiés ou non, émanant des établissements d'enseignement et de recherche français ou étrangers, des laboratoires publics ou privés.

New Journal of Physics
The open-access journal for physics

Forward THz radiation emission by femtosecond filamentation in gases: theory and experiment

C D Amico[1], A Houard[1], S Akturk[1], Y Liu[1], J Le Bloas[2], M Franco[1], B Prade[1], A Couairon[3], V T Tikhonchuk[2] and A Mysyrowicz[1,4]

[1] Laboratoire d'Optique Appliquée, ENSTA, Ecole Polytechnique, CNRS UMR 7639, Palaiseau, 91761 France
[2] Centre Laser Intenses et Applications, Université Bordeaux 1, CNRS, CEA, Talence, 33405 France
[3] Centre de Physique Théorique, CNRS, Ecole Polytechnique, F-91128 Palaiseau, France
E-mail: ciro.damico@ensta.fr and Andre.Mysyrowicz@ensta.fr

New Journal of Physics **10** (2008) 013015 (18pp)
Received 27 September 2007
Published 17 January 2008
Online at http://www.njp.org/
doi:10.1088/1367-2630/10/1/013015

Abstract. A transition–Cherenkov electromagnetic emission by a femtosecond laser pulse propagating in a self-induced plasma channel in air has been very recently proposed as mechanism for production of terahertz (THz) radiation in the forward direction. In this paper, we study in detail the theory of the transition–Cherenkov process. The theoretical model is developed and compared with recent experimental results for several gases.

[4] Author to whom any correspondence should be addressed.

© IOP Publishing Ltd and Deutsche Physikalische Gesellschaft

Contents

1. Introduction **2**
2. Femtosecond laser filamentation **3**
3. Theoretical model for forward THz emission **4**
3.1. Plasma wave excitation in the wake of laser pulse 5
3.2. Electromagnetic emission from the plasma wake 6
4. Forward THz generation and measurement in air **9**
4.1. Remote forward THz source created in air by focusing TW laser pulses 10
5. Experimental results on forward THz emission by filamentation in noble gases **12**
6. Comparison of the conversion efficiencies of forward THz emission in noble gases and in air **13**
7. Forward THz emission and above threshold ionization (ATI) processes **14**
8. Conclusions **16**
Acknowledgment **17**
References **17**

1. Introduction

The region of the electromagnetic spectrum with frequencies between 10^{11} and 10^{13} Hz, commonly called the terahertz (THz) region, has remained unexplored for a very long time due to the lack of efficient generation and detection techniques. Heterodyne techniques, commonly used to detect microwave radiation (10^9–10^{10} Hz), could not be used to detect THz radiation, because of the lack of THz local oscillators. Worse, 'THz photons' are not energetic enough to induce photoelectric effects in materials, making photoelectric effect based detection techniques unpractical.

This situation has changed in the last few decades and the THz domain has witnessed significant attention and improvements. New techniques have been developed for both generation and detection of THz radiation. Among other methods, the optical rectification process in non centro-symmetric crystals has been shown to produce THz radiation. In this method, the fundamental frequency ω of an infrared femtosecond laser pulse (duration $\tau_L \approx 100$ fs) is down-converted to the THz frequency ω' via the second-order susceptibility: $P_i(\omega') = \chi^{(2)}_{ijk}(\omega', \omega' + \omega, -\omega) E_j(\omega' + \omega) E^*_k(\omega)$. This conversion gives a coherent THz pulse, since the Fourier transform of the rectified pulse envelope yields a carrier frequency of about 10 THz [1]. For this process, ZnTe and GaAs crystals are mostly used, thanks to their favorable transmission and phase matching behaviors.

Optical rectification can generate THz radiation in centro-symmetric media, such as gases, as well. In this case, the fundamental frequency is mixed with the second harmonic, in a third-order process: $P_i^{(3)0}(t) \propto \chi^{(3)}_{ijkl} E_j^{2\omega}(t) E_k^{\omega}(t) E_l^{\omega}(t)$. Likewise, in an inverse process, the THz radiation can be mixed with the fundamental and give rise to second-harmonic generation, yielding a method for detection: $P_i^{(3)2\omega}(t) \propto \chi^{(3)}_{ijkl} E_j^{\omega}(t) E_k^{\omega}(t) E_l^{0}(t)$ [2, 3]. This detection and generation scheme is particularly attractive since it could use ubiquitous air for both generation and detection, with a very good efficiency. A THz signal with estimated field strength greater

than 400 kV cm^{-1} has been recently reported [4]. Note that in this case, the high conversion process in the gas needs the presence of a plasma.

The THz generation via optical rectification in gases has some limitations. Firstly, it requires precise alignments; making its use a difficult task. Secondly, due to water vapor, the THz radiation is significantly attenuated during propagation in air. This poses a challenge for long distance propagation and remote detection.

Generation of radial THz radiation by filamentation of femtosecond laser pulses in air has also been predicted [5]–[7] and experimentally demonstrated [8] in recent years. The mechanism that gives rise to the radial THz radiation by a filament has been a controversial subject. Cheng *et al* [5] proposed that the radial THz emission is due to the plasma oscillations induced by the pulse radiation pressure and the emission is coherent. According to Sprangle *et al* [6], however, the emission is due to some components of the pulse ionization front, which have superluminal velocities and give rise to Cherenkov radiation. One also expects the THz emission to be coherent in this case. Another model, as described in [7], is based on the scattering of electrons by ions in the plasma, and predicts an incoherent bremsstrahlung-like THz radiation. In addition to the predicted temporal coherence, D'Amico *et al* [9] demonstrated that the radially emitted THz radiation from the filament has very good spatial coherence properties.

Despite the controversies on the explanation of its mechanism, generation of THz radiation by filamentation received immediate attention since it requires almost no alignment; and more importantly since it potentially resolves the challenge of transmitting THz over long distances. The filaments can be generated over controllable distances, up to several hundreds of metres in air, by adjusting the input pulse parameters [10, 11]. Transmitting the filament consequently transmits the accompanying THz radiation, as well.

In a recent work [12], a novel THz emission process from femtosecond filaments in air has been reported. As opposed to the earlier works, which showed radially emitted THz from filaments, this process gives rise to a relatively collimated emission in the laser propagation direction. The physical mechanism behind this process is attributed to combined transition–Cherenkov radiation.

In this work, we present a comprehensive theoretical analysis and experimental study and of the forward THz emission from filaments. We begin by a brief summary on filamentation, long distance laser propagation and forward THz generation. We then present a detailed discussion of the theoretical model explaining the THz emission as transition–Cherenkov radiation. Next, we present experimental results on THz generation from filaments in air and noble gases (argon, krypton and xenon) and compare the corresponding conversion rates. Due to the involvement of the electron collision cross-section in the process, the highest conversion efficiency is found in xenon, in agreement with the theoretical model. We also used the relative conversion efficiencies to estimate the kinetic energy of electrons in the multiphoton ionization process during filamentation.

2. Femtosecond laser filamentation

Filamentation denotes a peculiar phenomenon related to the propagation of a beam of light through a medium without apparent diffraction. Counteracting the natural spreading of the beam is possible with intense laser pulses owing to the optical Kerr effect, which causes a change of the refraction index in the medium proportional to the beam intensity. The core of the beam,

more intense than the wings, induces a spatial phase profile equivalent to that of a focusing lens, resulting in self-focusing of the beam. In contrast with a lens, however, the effect is cumulative but self-focusing overcomes diffraction and eventually leads to a catastrophic collapse only if the beam power exceeds a critical threshold.

With the advent of chirped pulse amplification [13], ultrashort laser pulses became easily available with peak powers exceeding this threshold. Filamentary propagation of laser pulses in air was observed in 1995 [14] and led to numerous works since this observation. For a review about filamentation process see [15].

One of the distinguishing features of filaments is their ability to generate tenuous plasmas in the wake of the propagating pulse, which in turn modifies the narrowband laser pulse into a broadband pulse [16, 17]. This opens up the possibility of a wholly new set of applications ranging from the pulse compression and generation of extreme ultraviolet radiation [18]–[21] to the remote generation of THz radiation [12]. In addition, filaments have numerous interesting properties. For instance, the plasma strings can be concatenated to enlarge their total length [22]; filaments can be amplified in suitable media [23, 24]; the combination of plasma string generation with the organization of multiple filaments into rings or arrays [25] was predicted to serve as a photonic crystal to guide radar signals [26].

Although the initial interpretation of a balance between the Kerr self-focusing and both the self-attenuating natural diffraction and plasma-induced defocusing is still a debated topic (see for instance, the recent interpretation based on the excitation of dispersion- and diffraction-free modes [27]–[34]), the conditions to control the filamentation process and the generation of a plasma string with given features from terawatt laser pulses are well identified at least in the laboratory, making the option of using filaments as sources of THz radiation very attractive.

3. Theoretical model for forward THz emission

It has been predicted in [5] that the plasma channel formed by the laser pulse propagating in air should emit THz radiation perpendicularly to the filament axis. The underlying physical process was interpreted as originating from the radiation pressure of the laser pulse that induces longitudinal plasma oscillations, with frequency equal to the plasma frequency. For an electron density typically obtained in filaments, $n_e = 10^{16}\,\mathrm{cm}^{-3}$, the plasma frequency lies in the THz region, $\omega_{pe} = \sqrt{n_e e^2/m_e \varepsilon_0} \approx 6 \times 10^{12}\,\mathrm{rad\,s}^{-1}$. Sprangle *et al* [6] have highlighted the main role of the ponderomotive force in the THz emission by plasma strings. In their model, the radial THz electric field is estimated to be about $5\,\mathrm{kV\,cm}^{-1}$, in the near field.

Here, we review the predictions of our theoretical model which provides the basis for interpreting the measurements of the radial as well as the forward components in the angular diagram of THz emission. Our model predicts a conical THz emission by a Cherenkov-like process of the electric current moving in the plasma channel behind the ionizing laser pulse. Similarly to the Cherenkov emission of an electric charge moving faster than the light group velocity, the emission is localized on the surface of a cone oriented in the propagation direction, it has a radial polarization, and the source size is much smaller than the emission wavelength. However, there are two main differences in the process: firstly, there is no net charge in the plasma channel. The ponderomotive force of the laser pulse produces the charge separation, but the wake is neutral as a whole, i.e. the moving source in our case is a dipole-like structure. The interference between the emissions of the positive and negative charges decreases the emission efficiency, but does not suppress it completely. Secondly, the THz source in our case is generated

even if the velocity of the ionization front is exactly the light velocity. Therefore, the radiation would not exist in an infinite plasma string; it is actually generated due to the finite length of the filament, which also defines the emission angle. In that sense it resembles transition radiation but it is more efficient, as we will see later in this section. Note finally that the refraction index of the weakly ionized air is slightly smaller than 1, making the source slightly superluminal. Therefore, the THz radiation is also partly generated by a Cherenkov-like mechanism, although superluminality is not strictly necessary, as in the Sprangle model [7].

Our theoretical development contains two parts. Firstly, we recall the theory of the plasma wave generation in the plasma channel and present estimates of it for the parameters of our experiment. Secondly, we present a model of the electromagnetic emission of the moving plasma wave from the channel and estimate the spectrum and the energy of the emitted signal.

3.1. Plasma wave excitation in the wake of laser pulse

Let us consider a motion of electrons in the plasma channel created by the laser pulse. According to the studies on filamentation of ultra short laser pulses in air [15], we consider an infrared laser pulse of duration ∼100 fs, focused in a spot of radius ∼100 μm and creating a plasma channel of radius ∼40–60 μm and a few cm or a few tens of cm long. The self-guided pulse is shaped like a pancake since its length ∼10–15 μm is shorter than both its radius and the plasma column radius; therefore, it is sufficient to describe the motion of electrons in a one-dimensional model, along the laser propagation axis z. The longitudinal electric field E_z created in the plasma string is described by the wave equation

$$\partial_t^2 E_z + \nu_e \partial_t E_z + \omega_{pe}^2 E_z = S_z, \tag{1}$$

where ν_e is the electron collision frequency, $\omega_{pe} = \sqrt{e^2 n_e / m_e \varepsilon_0}$ is the electron plasma frequency and the source term, S_z, has been derived by Sprangle *et al* [6]:

$$S_z(r, z, t) \approx \frac{e\omega_{pe}^2}{2\varepsilon_0 m_e \omega_0^2 c}\left(\frac{2\nu_e}{c} + \frac{2}{c\omega_{pe}^2}\frac{\partial \omega_{pe}^2}{\partial t} - \frac{\partial}{\partial z}\right) I_L, \tag{2}$$

where I_L is the laser pulse intensity. The dominant terms in the source are the first term proportional to the collision frequency, which accounts for the radiation pressure created by the laser pulse and the third term involving the spatial derivative, which accounts for the ponderomotive force. The temporal variation of the electron density takes place only in the head of pulse and can be neglected. The general solution to equation (1) in the reference frame of the laser pulse, $\tau = t - z/c$, takes the following form:

$$E_z(\tau) \propto \frac{e\omega_{pe}}{2\varepsilon_0 m_e c^2 \omega_0^2} \int_0^{\tau_L} d\tau' e^{-\nu_e(\tau-\tau')/2} \sin\left(\omega_{pe}(\tau - \tau')\right)\left(\frac{\partial}{\partial \tau'} + 2\nu_e\right) I_L(\tau'). \tag{3}$$

Here, we supposed that the electron collision frequency is small compared to the plasma frequency, $\nu_e < \omega_{pe}$. An example of the plasma wave electric field created in the wake of a laser pulse is shown in figure 1 for typical parameters of our experimental conditions: $\nu_e = 1.3\,\mathrm{ps}^{-1}$, the laser pulse duration $\tau_L = 120$ fs and $\omega_{pe} = 10\,\mathrm{ps}^{-1}$.

The plasma wave pulse is rather short, it contains 2–3 oscillations and damps out within 1 ps time. The maximum amplitude is about 200 V cm^{-1} for a laser pulse intensity

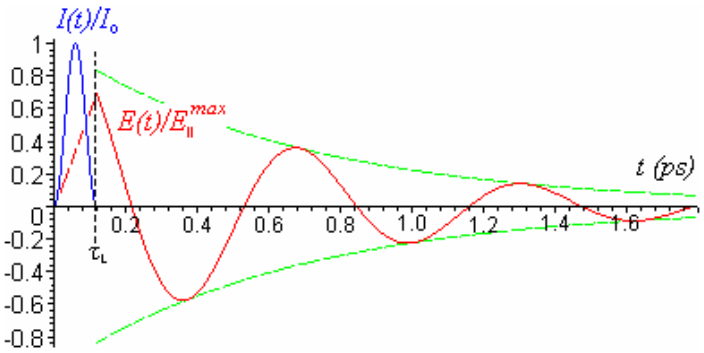


Figure 1. Temporal profile of the longitudinal electric field in the plasma (red curve) created in the wake of a sine shaped laser pulse, the profile of which is shown in blue curve.

of 24 TW cm^{-2}. The general form for the maximum field amplitude can be calculated from equation (3) for the sine laser pulse intensity, $I_{\mathrm{L}}(\tau) = I_0 \sin^2(\pi\tau/\tau_{\mathrm{L}})$. Then $E_z^{\max}$ becomes:

$$E_z^{\max} = \frac{2\pi^2 e\omega_{\mathrm{pe}} I_0 \sin(\omega_{\mathrm{pe}}\tau_{\mathrm{L}}/2)}{\varepsilon_0 m_{\mathrm{e}} c^2 \omega_0^2 (4\pi^2 - \omega_{\mathrm{pe}}^2 \tau_{\mathrm{L}}^2)}. \tag{4}$$

The optimum condition for the plasma wake excitation $\omega_{\mathrm{pe}}\tau_{\mathrm{L}} = 2\pi$ is achieved for the pulse duration that equals the plasma wave period, $\mathrm{E}_z^{\max} = \pi e\omega_{\mathrm{pe}} I_0/4\varepsilon_0 m_{\mathrm{e}} c^2 \omega_0^2$. It can reach a few kV cm^{-1} for our parameters. From the maximum amplitude of the wake field, the total pulse energy transferred to the plasma wave can be estimated as $W_{\mathrm{p}} \approx \pi\rho_0^2\varepsilon_0 |E_z^{\max}|^2 L$, which is of the order of 10^{-10} J, much less than the energy deposited for the ionization.

The calculation of the electromagnetic emission is performed from the Fourier spectrum of the electric current associated with this plasma wave, $j_z(\omega) = \mathrm{i}\varepsilon_0\omega E_z(\omega)$, which can be written as:

$$j_z\omega = -\frac{e\omega\omega_{\mathrm{pe}}^2\,(\omega + 2\mathrm{i}\nu_{\mathrm{e}})}{2m_{\mathrm{e}}c^2\omega_0^2\left(\omega^2 - \omega_{\mathrm{pe}}^2 + \mathrm{i}\nu_{\mathrm{e}}\omega\right)} I_\omega, \tag{5}$$

where I_ω is the Fourier spectrum of the laser pulse intensity. The current spectrum has a pronounced maximum at the plasma frequency, and it behaves as a linear function for low frequencies, $\omega \ll \omega_{\mathrm{pe}}, \nu_{\mathrm{e}}, \tau_{\mathrm{L}}^{-1}$:

$$j_z\omega = \frac{\mathrm{i}e\omega\nu_{\mathrm{e}}\tau_{\mathrm{L}}}{2m_{\mathrm{e}}c^2\omega_0^2} I_0. \tag{6}$$

This is the frequency domain corresponding to our measurements. It is important to notice that the current in this spectral range is proportional to the electron collision frequency and the laser pulse flux, $I_0\tau_{\mathrm{L}}$, but does not depend on the plasma density.

3.2. Electromagnetic emission from the plasma wake

In this derivation, we are following the recent publication by Zheng *et al* [35] where the effect of the finite orbit length on the Cherenkov emission of a charged particle has been considered.

The radiated field can be calculated directly from the well-known expression for the vector potential $\boldsymbol{A}$ created by a current $\boldsymbol{j}$ [36]:

$$\boldsymbol{A}(\boldsymbol{r}, t) = \frac{\mu_0}{4\pi} \int \mathrm{d}^3 r' \frac{\boldsymbol{j}(\boldsymbol{r}', t')}{|\boldsymbol{r} - \boldsymbol{r}'|}, \qquad t' = t - \frac{|\boldsymbol{r} - \boldsymbol{r}'|}{c}, \tag{7}$$

where t–t' is the time for the field to travel from the point of emission to the point of observation. By considering the far field, $r \gg r'$, c/ω, this formula takes a simple form for the Fourier component of the vector potential

$$\boldsymbol{A}_\omega(\boldsymbol{r}) = \mu_0 \frac{\mathrm{e}^{\mathrm{i}kr}}{4\pi r} \boldsymbol{j}_{\omega,k}, \tag{8}$$

where $\boldsymbol{k} = \boldsymbol{n}\,\omega/c$, is the field wave vector and $\boldsymbol{n}$ is the unit vector in the radial direction. (In fact, we measured the signal at a distance of the order of 10 cm, comparable to the length of the plasma channel $r \approx r'c/\omega$. The predictions of the theoretical model will be therefore compared only qualitatively with experimental results.)

For our case, where the current is in the axial direction, the magnetic field, $\boldsymbol{B} = \mathrm{curl}\,\boldsymbol{A}$, has only the azimuthal component, $\boldsymbol{B}_\varphi = -\mathrm{i}kA_z \sin\theta$. Correspondingly, the radiation field is zero on the laser axis, $\theta = 0$. The electric field is then perpendicular to $\boldsymbol{n}$ and $\boldsymbol{B}$, i.e. the emission has a radial polarization.

Since the radius of the plasma column ρ_0 is smaller than the emission wavelength, one can assume a δ-function distribution of the current in the radial direction. From the axial current distribution in the pulse frame given by equation (1), the Fourier component of the current reads:

$$j_{z,\omega}(\boldsymbol{\rho}, z) = \pi\rho_0^2 \delta(\rho) \mathrm{e}^{\mathrm{i}\omega z/c} j_z(\omega, z). \tag{9}$$

While taking the spatial Fourier transform of the current one has to account for the finite length of the emission zone L in the axial direction. The energy spectral density of electromagnetic radiation emitted in the unit solid angle then reads:

$$\frac{\mathrm{d}^2 W}{\mathrm{d}\omega\,\mathrm{d}\Omega} = \frac{cr^2}{\pi\mu_0} |B_\omega|^2 = \frac{|j_z(\omega)|^2}{4\pi\varepsilon_0 c} \frac{\rho_0^4 \sin^2\theta}{(1-\cos\theta)^2} \sin^2\left(\frac{L\omega}{2c}(1-\cos\theta)\right). \tag{10}$$

This constitutes our principal result describing the angular and spectral distribution of the radiation as a product of two factors. The frequency spectrum is shown in figure 2 (left). It has a maximum at the plasma frequency, corresponding to a few THz, and a broad low frequency tail decreasing as ω^{-2}. The angular distribution contains multiple lobes, the angular positions of which are defined by the condition: $4L \sin^2\theta/2 = N\lambda$. Here, $\lambda = 2\pi c/\omega$ is the emission wavelength and N is an integer. The lobe $N = 1$ is the strongest and corresponds to the cone opening angle

$$\theta \approx \sqrt{\lambda/L}. \tag{11}$$

It is shown in figure 2 (right) for the case $L\omega/c = 200$.

The energy spectral density of the total emission follows from equation (10) by integrating over angles

$$\frac{\mathrm{d}W}{\mathrm{d}\omega} = \frac{\rho_0^4}{2\varepsilon_0 c} |j_z(\omega)|^2 \left[\gamma - 1 + \ln 2L\omega/c\right], \tag{12}$$

where γ is the constant of Euler. In fact, the term $\gamma - 1$ accounts for the emission in the first lobe and the logarithmic term is the contribution from other angles, which is much less intense than

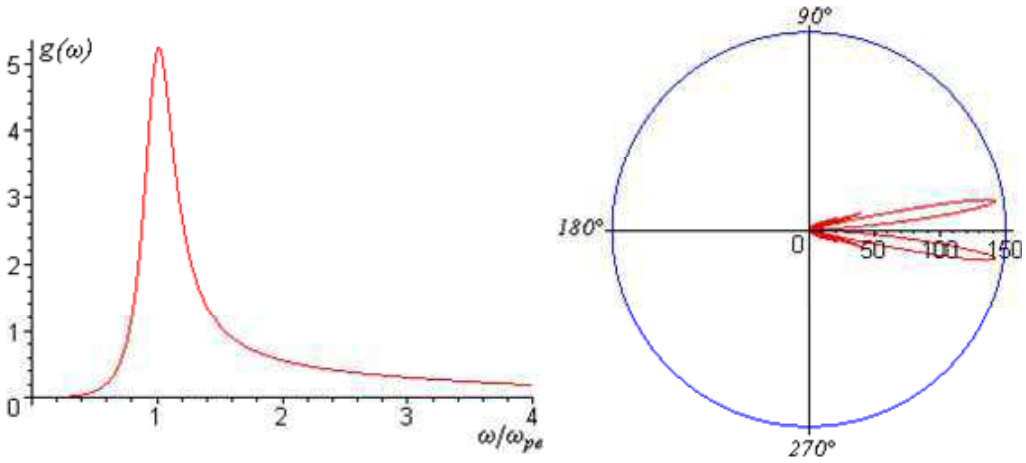


Figure 2. Spectrum (left) and the angular distribution (right) of the electromagnetic emission.

the main conical emission in the first lobe as it is distributed over all directions. In this respect, the model presented above for the conversion of plasma waves into electromagnetic waves also explains the emission observed at large angles, $\theta \approx \pi/2$ [6]. As a consequence, the energy of the electromagnetic emission within the cone is independent of the filament length, which defines only the emission angle. These features are quite different from those of the standard Cherenkov emission for which the energy is proportional to the length of the particle trajectory.

According to equations (6) and (12), the energy spectral density of the electromagnetic emission in the long wavelength domain is proportional to the square of the laser pulse energy and the square of the electron collision frequency. The emission efficiency should therefore increase for gases which contain big atoms, such as xenon where the effective cross-section of elastic electron collisions is larger than in air and in other noble gases.

Finally, by taking the integral in equation (12) over frequency one can estimate the total energy of the electromagnetic emission:

$$W = \frac{r_e \omega_{pe}^6}{16 m_e c^3 \omega_0^4 \nu_e} \left(I_0 \tau_L \pi \rho_0^2\right)^2 \left[\gamma + \ln\left(2L\omega_{pe}/c\right) - 1\right], \tag{13}$$

where $r_e = \mu_0 e^2/4\pi m_e$ is the classical electron radius. The emitted energy is proportional to the square of the laser pulse energy, the third power of the electron density and it is inversely proportional to the electron collision frequency. The spectrum width of the THz emission is smaller for gases with a low electron collision frequency.

For the parameters of our experiment, the total electromagnetic energy in the THz domain is predicted to be relatively small, about 10^{-14} J, corresponding to the emission efficiency of about 10^{-11}, which is actually due to a low conversion of the laser beam into the plasma wake. In the present example, about 2% of the plasma wave energy is converted into the electromagnetic emission. This is a quite reasonable number if one accounts for the high electron collision rate and therefore, for a strong collisional dissipation of the plasma wave.

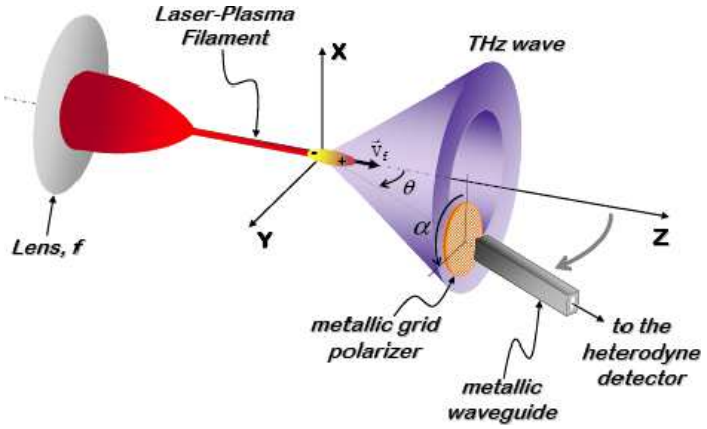


Figure 3. Experimental set-up used for THz generation and measurement.

4. Forward THz generation and measurement in air

The experimental set-up used for the study of THz generation by filaments is shown in figure 3. The laser source is a Ti:sapphire CPA (chirped pulse amplification) system operating at 10 Hz and delivering pulses of 150 fs duration. A single filament is formed by focusing 4 mJ (∼27 GW) femtosecond laser pulses in air using a 2 m focal lens. In the experiment, the central part of the beam traversing the lens is selected by means of a 5 mm diameter diaphragm, yielding a super-Gaussian spatial profile. We detect a specific spectral component of the broadband THz radiation emitted by the plasma filament with a heterodyne detector operating either at 91 or 110 GHz (0.1 THz).

The predictions of the theoretical model have been experimentally verified by measuring the forward THz radiation in air in this low frequency range. Concerning the polarization properties, the direction of the THz electric field is perpendicular to the detection axis, it lies on the plane common to both detection and filament axes, and it does not depend on the laser pulse polarization direction. By symmetry considerations, we conclude that the radiation is radially polarized, as predicted by the transition–Cherenkov model.

Most of the measurements were done with the heterodyne detector at 0.1 THz, but we also recently measured the spectral distribution of the produced THz pulse between 0.1 and 3 THz with calorimetric detection [37]. The THz forward radiation from the filament was collected with an off-axis parabola, and the collimated THz beam was sent to the bolometer at 4 K (see description of the detector in [38]). By inserting several calibrated band-pass and low-pass filters we were able to confirm that most of the THz pulse energy is emitted in the spectral region above 1 THz, and that its spectral distribution follows qualitatively the prediction of the theoretical model.

At low frequencies the general formula (10) can be approximated by:

$$\frac{\mathrm{d}^2 W}{\mathrm{d}\Omega\,\mathrm{d}\omega} \propto \frac{E_\mathrm{f}^2 \nu_\mathrm{e}^2 \omega^2}{\theta^2} \sin^2\left(\frac{L\theta^2}{4c}\omega\right), \tag{14}$$

where E_f is the energy contained in the self-guided pulse. This formula describes the THz angular emission diagram at low frequencies. The aperture angle of the emission cone is inversely proportional to the square root of the plasma channel length, as was previously pointed out. We measured the plasma channel length, under different focusing conditions, by recording

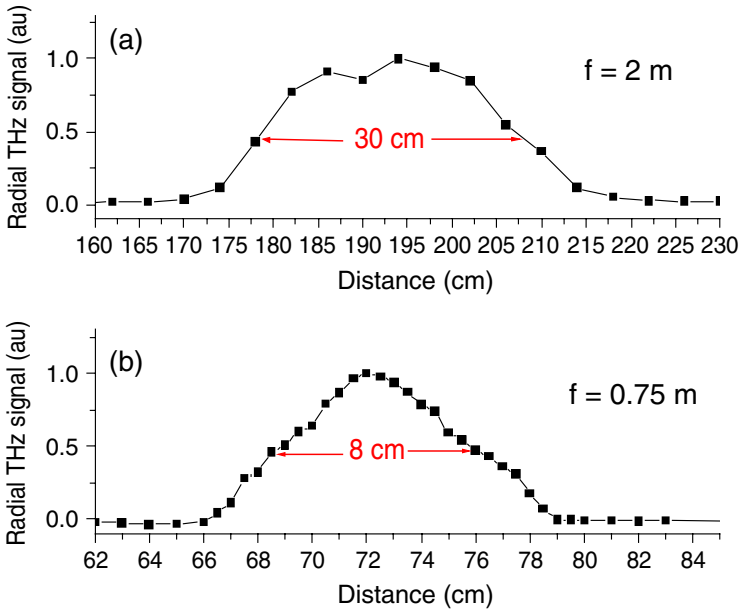


Figure 4. Radial THz signal as function of the propagation distance, measured along the filament for two different focal length lenses: $f = 2$ m (a) and $f = 0.75$ m (b). The full width at half maximum (FWHM) is the length of the obtained plasma channels.

the radial THz emission, under the reasonable assumption that the locally measured emission requires the presence of plasma. In figure 4, the results of measurements are shown for two different focal lengths, 2000 and 750 mm. In the first case, the self-guided laser pulse creates a 30 cm long plasma channel and in the second case it is 8 cm.

For each set of focusing conditions we have recorded the angular diagram by rotating the detector around a fixed point along the filament axis, as shown in figure 3. We have compared the measured and calculated emission diagrams for different lengths of filament, finding a very good agreement between theory and experiment. In particular, the law $\theta \approx \sqrt{\lambda/L}$ for the maximum emission angle has been experimentally verified. In figure 5, we show the comparison between the measured and calculated emission diagrams for an 8 cm long filament.

4.1. Remote forward THz source created in air by focusing TW laser pulses

To test the potential of this forward THz conical emission to reach high intensities on distant targets, we have also measured the THz emission from filaments generated with the Teramobile laser [39]. In this case, the pulse peak power was 2 TW. The laser pulse was focused by means of a telescope with the focal length of 20 m. The laser beam splits in a multi-filamentary structure before collapsing in a large bundle, which generates a 5 mm diameter and 4 m long plasma column, around the focus. The measurement of forward THz emission was performed by means of the 0.1 THz heterodyne detector. We obtained in this case a strong THz signal and the corresponding emission angular diagram is shown in figure 6. The detector was placed 2.5 m away from the rotation point along the laser axis. Due to the experimental difficulties resulting from the long plasma channel and large beam size, we measured the THz radiation only on one

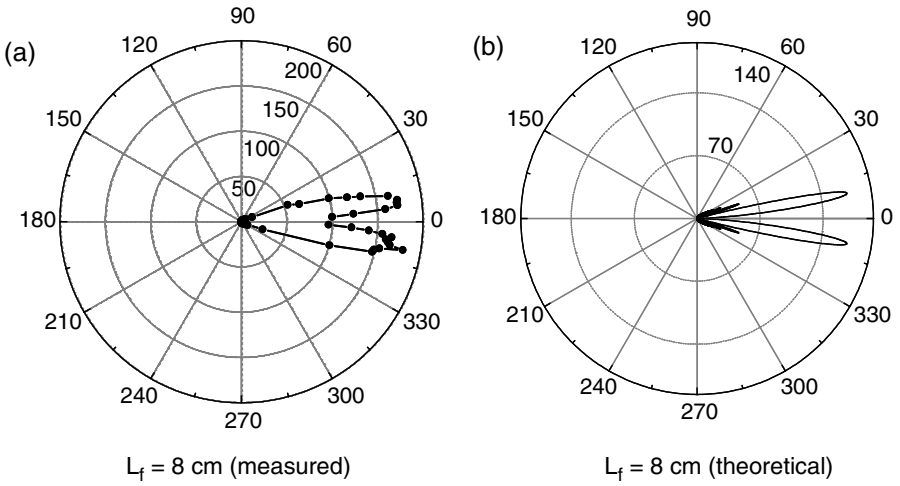


Figure 5. Comparison between experimental (a) and theoretical (b) THz emission angular diagrams for an 8 cm long filament.

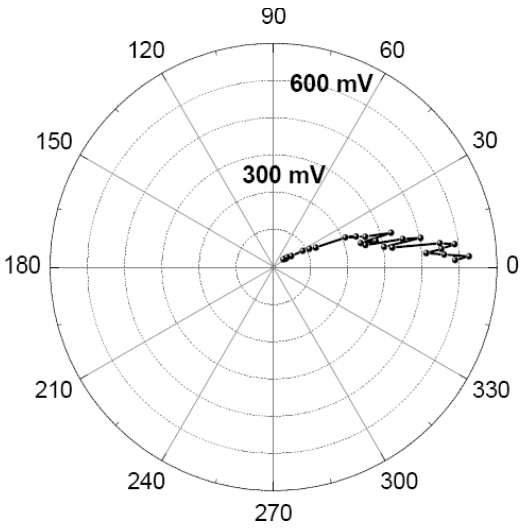


Figure 6. Experimental angular diagram (measured only between 0° and 180°) of THz radiation created at long distance (20 m) with a TW laser (Teramobile).

side of the beam. Note that, overall, the measured angular distribution matches the theoretical model. The fine structures result from the fact that for the long plasma channels involved, the measurement position is not quite in the far-field. Taking into account the measurement position, by comparing the signal levels for the pulse peak powers of 27 GW shown above and 2 TW, we estimate, for the latter case, a forward emission with energy of two to three orders of magnitude stronger than the former. The energy needed for the pulse to create a large plasma column is about one to two orders of magnitude larger than in the case of one filament, where we created a 100–200 μm large plasma column. Now, following the transition–Cherenkov model, the radiated power in unit solid angle is proportional to the square of the energy of the self-guided pulse that creates the plasma (equation (14)), therefore we expect the radiation to be

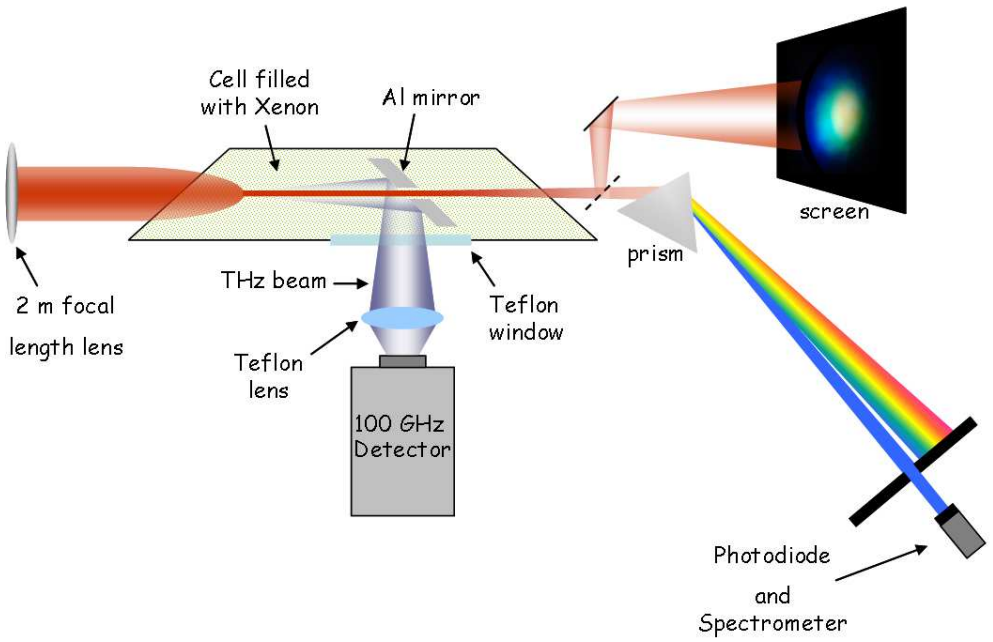


Figure 7. Experimental set-up used to detect, at the same time, the THz emission and the conical emission of the filament in gases.

between 100 and 1000 times stronger in the case of a large plasma column. A study of the polarization properties of the emitted radiation showed a radial polarization, as in the previous experiments.

5. Experimental results on forward THz emission by filamentation in noble gases

In this section, we present our experimental study of the THz emission from filamentation in noble gases. In most of our experiments, we used xenon, except that at the end of this section we present a comparison between xenon, argon and krypton. Figure 7 shows the experimental set-up that we used for the measurements in this section. The laser system is a Ti:sapphire CPA, which can deliver pulses with energies up to 15 mJ (at 100 Hz), with duration of ∼40 fs, centered at 800 nm wavelength. The pulses were focused with a 2 m focal length lens into a 1.5 m long gas cell. The gas pressure was kept around 1 atm. In order to avoid the absorption of the forward THz radiation by the exit window, we used a 45° aluminium mirror, with a half-circle hole at the top, to reflect the THz beam. The reflected half of the THz cone then passes through the Teflon wall of the cell, and is detected by the heterodyne 0.1 THz detector.

We first investigate the dependence of the THz radiation on the pulse energy. The integration over the solid angle of the equation (14) gives:

$$\Delta W \propto E_f^2 \nu_e^2 \nu^2 \ln\left(\frac{2\pi L \nu}{c}\right) \Delta\nu, \tag{15}$$

where $\nu = 0.1$ THz, is the signal frequency and $\Delta\nu = 6$ GHz is the bandwidth of our heterodyne detector. As the intensity of the laser pulse in the filament is defined by the filamentation process, we conclude that the efficiency of the forward THz emission should be proportional to the square

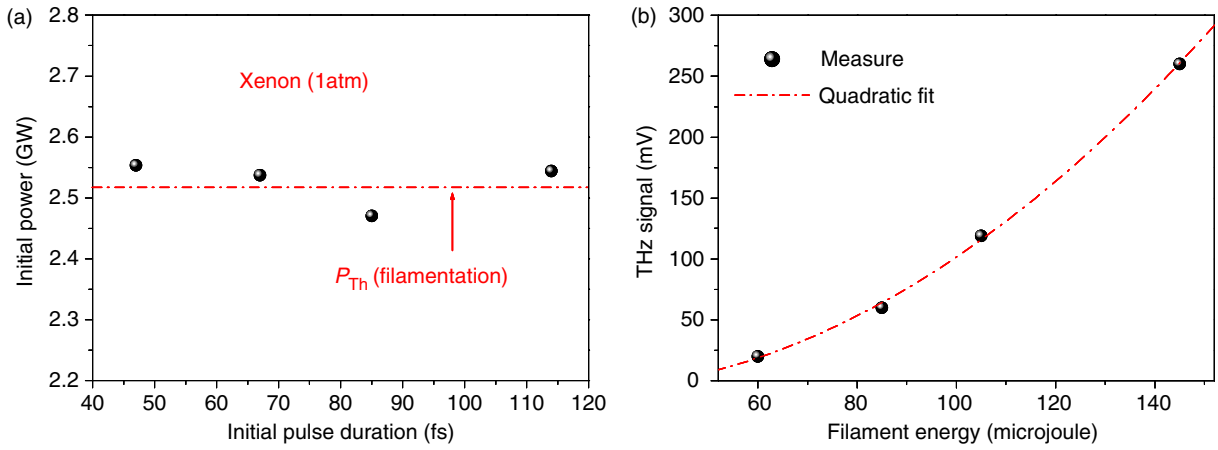


Figure 8. Measured THz signal (back dots) as a function of the filament energy, along with quadratic fit (dash-dotted line).

of the pulse energy, the square of the electron–neutral collision frequency and the logarithm of the filament length.

In order to examine the agreement of the theory with the experimental results, we varied the pulse duration in the range 40–120 fs, by adjusting the bandwidth at the compressor part of the CPA system, and kept the input power around the threshold for filamentation in xenon (about 2.5 GW) (see figure 8(a)). For different durations we measured the input and output pulse energies and found nearly constant transmission in accordance with Dubietis *et al* [40]. For the mono-atomic gases involved, the critical power does not change with the pulse duration. Thus changing the duration of the input pulse allowed us to change the energy contained in the filament. In figure 8(b), we present the measured THz signal as a function of the filament energy and observe a quadratic dependence, in accordance with the theory (see equation (15)).

In these experiments, we also observed a bright 'blue spot' after filamentation, emitted in the laser direction, but slightly off-axis (see inset of figure 9). The spectrum of the spot is centered at a wavelength of 400 nm, corresponding to the second harmonic of the input signal. Since the gases that we use are all centro-symmetric, we attribute this second harmonic generation (SHG) to the mixing of the generated THz signal with the fundamental, in a third order nonlinear process. This process can be described with the polarizability: $P_i^{(3)2\omega}(t) \propto \chi_{ijkl}^{(3)} E_j^{\omega}(t) E_k^{\omega}(t) E_l^{0}(t)$ [41]. During the filamentation, the laser pulse can split into multiple pulses; hence, the THz generated at the peak of the pulse can interact with the trailing portion of the pulse. To confirm this, we spatially and spectrally filtered the SHG, and measured its relative strength with respect to the strength of the emitted THz. As shown in figure 9, we observe that the SHG signal is linearly proportional to the THz, as expected from the equation above.

6. Comparison of the conversion efficiencies of forward THz emission in noble gases and in air

In order to study the dependence of THz generation on the electron collision frequency, we measured the forward THz signal emitted from filaments in xenon, argon, krypton and air, all at atmospheric pressure. For each case, we also measured the energy in the filament coming out of

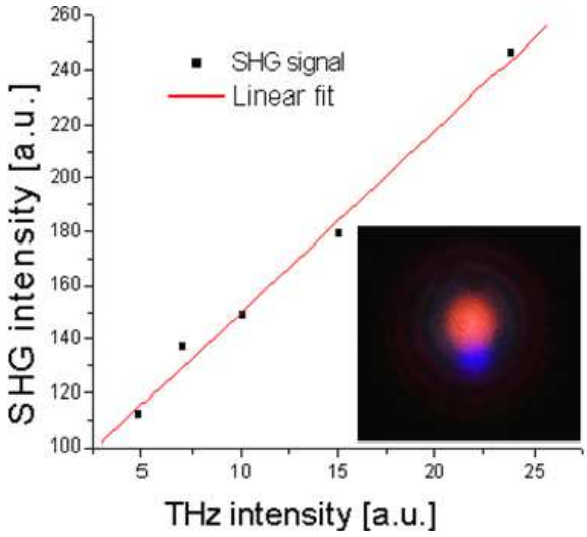


Figure 9. SHG signal versus the THz signal. The linear dependence of these two signals is an indication of SHG by the third-order mixing of the fundamental and THz pulses. The inset is a photographic picture of the conical emission coming from the filament. The blue spot that gives SHG signals is emitted off-axis and exhibits a 400 nm centered frequency spectrum.

Table 1. THz signal and filament energy measured for four different gases.

Gas ($p = 1$ atm)	THz signal (mV)	Filament energy (μJ)
Air	90	700
Ar	51	410
Kr	61	300
Xe	44	100

the cell by selecting the core with an aperture. In table 1, we show the measured values of the THz signal and the filament energy.

In light of the theoretical considerations presented above, one can assume the same temporal length of the emitted THz pulse in the different noble gases. Therefore, the relative conversion rates can be estimated by dividing the THz signal by the energy in the filament. From table 1, we can find the following ratios between the conversion rates: $\eta_{\mathrm{Ar}}/\eta_{\mathrm{Air}} \approx 1$, $\eta_{\mathrm{Kr}}/\eta_{\mathrm{Air}} \approx 1.6$ and $\eta_{\mathrm{Xe}}/\eta_{\mathrm{Air}} \approx 3.4$. These relative conversion ratios qualitatively match our expectation from the theory, as equation (15) predicts that the THz energy increases with the electron collision cross-section, as discussed in more detail below.

7. Forward THz emission and above threshold ionization (ATI) processes

In this section, we present a more detailed and quantitative study of the relative conversion efficiencies. We can express the electron–neutral atom collision frequency as $\nu_{\mathrm{e}} = n_{\mathrm{a}} \mathrm{v}_{\mathrm{e}} \sigma_{\mathrm{m}}$, where v_{e} is the mean electron velocity, n_{a} the gas neutral atom density and σ_{m} the momentum

transfer cross section (MTCS) of electrons. Equation (15) can therefore be written as:

$$\Delta W \propto E_f^2 n_a^2 v_e^2 \sigma_m^2 \nu^2 \ln\left(\frac{2\pi L_f \nu}{c}\right) \Delta\nu. \tag{16}$$

The density of neutral atoms, for a given pressure, is the same for all considered gases. The power of the THz emission has a logarithmic and therefore weak dependence on the filament length, L_f, hence can be neglected. As a result, the ratio between the emitted THz power and the squared filament energy is only proportional to σ_m^2 and the squared average electron velocity, i.e. the averaged electron kinetic energy, $T \propto v_e^2$. Therefore, one can compare the electron MTCSs for different gases by writing:

$$\frac{\sqrt{T'}\sigma_m'(T')}{\sqrt{T}\sigma_m(T)} = \frac{E}{E'}\sqrt{\frac{S'_{THz}}{S_{THz}}}, \tag{17}$$

where $\sqrt{T/T'} = v_e/v_e'$ and $S_{THz} \propto P_{THz}$ is the measured THz signal. We can write the electron kinetic energy for an s-photon ATI process [42] as $T = \sum_s \alpha_s(n+s)\eta\omega - (U_i + U_p)$, where $\eta\omega$ is the photon energy and s is the number of above-threshold photons. The integer number $n = \mathrm{mod}\left[\left(U_i + U_p\right)/\eta\omega + 1\right]$ is the minimum number of photons needed to ionize the atom. In this formula α_s is the probability of having an s-photon ATI process, U_i is the ionization energy of the atom or molecule and $U_p = e^2 I_L/2\varepsilon_0 m_e c\omega^2$ is the ponderomotive potential [43] given by the laser pulse intensity I_L. In general, in the range of intensities reached during filamentation, the ponderomotive potential is of the order of a few eV and cannot be neglected.

For a given pair of gases, the right-hand side of equation (17) is completely determined by the experimental values given in table 1. For the left-hand side, we assume that the averaged electron kinetic energy is nearly the same in all three noble gases. To justify this, we first recall that the intensity within a filament is clamped to a certain level given by equation (20) in [15]. The clamped intensity value in krypton is slightly higher than in xenon ($I \approx 3 \times 10^{13}\,\mathrm{W\,cm^{-2}}$ in krypton, $I \approx 1.2 \times 10^{13}\,\mathrm{W\,cm^{-2}}$ in xenon). On the other hand, from previous works on ATI processes [44] we can infer that in order to have electrons with the same average kinetic energy, one needs slightly higher intensity in krypton than in xenon because of the higher ionization potential of krypton. Hence, the difference in the clamped intensities approximately balances the average electron kinetic energies. The same argument also holds for the Xe/Ar and Kr/Ar pairs. The averaged electron kinetic energies in the considered gases are thus reasonably considered to be roughly the same; hence, we can write $T/T' \approx 1$. Equation (17) then becomes:

$$\frac{\sigma_m'}{\sigma_m}(T) \approx \frac{E}{E'}\sqrt{\frac{S'_{THz}}{S_{THz}}}. \tag{18}$$

Figure 10 shows a graphical examination of this equation. The MTCS ratios are plotted as functions of the electron kinetic energy, by comparing Xe/Ar (solid line), Xe/Kr (dotted line) and Kr/Ar (dash-dotted line) by using the MTCS values reported by Hunter *et al* [45] and by Frost and Phelps [46]. The values we measured are represented by dots in the graph of figure 10, and at the same time they determine the right-hand side of equation (18). The experimental data of figure 10 have fixed y-coordinates, while the electron kinetic energy (x-axis) is unknown. Therefore, the best fit of the measured points on the graphs gives a reasonably good estimation of the electron kinetic energy in our experiments.

As can be seen from figure 10, the best agreement is found for electron energies around 3 eV, but the zone between 2 and 4 eV still provides good results. We note that the zone

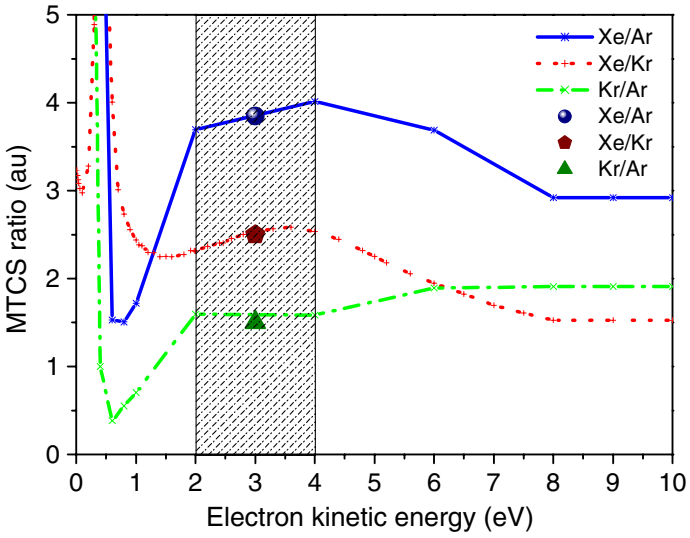


Figure 10. Graphical method used to examine equation (17). The solid, dotted and dash-dotted lines are the MTCS ratios for the comparison of Xe/Ar, Xe/Kr and Kr/Ar, respectively. The symbols represent our measurements. The symbols have *y*-axis values fixed by the measurement; they are translated along the *x*-axis (electron kinetic energy) in order to find the energy range in which we have the best agreement with the values reported in the literature. The best fit is found in the energy range 2–4 eV.

between 2 and 4 eV implies 1-photon and 2-photon ATI processes at a wavelength of 800 nm. Therefore, we conclude that 1-photon and 2-photon ATI processes can explain our experimental observation of forward THz emission during filamentation in rare gases. If one considers the intensity reached during filamentation processes in noble gases ($\sim 10^{13}$ W cm^{-2}), 1-photon and/or 2-photon ATI processes are expected with a high probability, as previously pointed out for longer pulse durations [44, 47].

We conclude that the forward THz emission is strongly tied to the ATI processes during the filamentation in rare gases. In particular, a high order ATI process, in the electron energy range 1–4 eV, should give a stronger forward THz emission. This can be particularly interesting for molecular gases, where the MTCS can exhibit resonances, due to the different rotational and vibrational states of molecules.

8. Conclusions

In this paper, we described the origin of the THz radiation from the filaments created by intense femtosecond laser pulses propagating in gases. Both the conical and radial components of THz emission have been attributed to the same effect, namely the transition–Cherenkov process. The space charge is generated at the pulse's peak intensity; the ponderomotive force of the laser field separates the charges, generating dipole-like structures, oscillating in the wake of the laser pulse. Since the ionization front moves with the laser at the speed of light, this gives rise to emission resembling transition and Cherenkov radiations. The theory of the transition–Cherenkov emission process has been developed and the spectrum and angular

distribution of the radiation has been calculated. THz experiments performed in air, xenon, krypton and argon have been compared with the theory. The THz radiation pattern is in excellent agreement with calculations. Furthermore, the THz emitted energy is shown to increase as the square of the laser pulse energy, as expected. Relative THz efficiencies measured in different gases depend on the electron–neutral atom collision frequency. From the relative efficiencies, it is possible to extract the initial electron kinetic energy during the multiphoton ionization process. It is shown that ATI plays an important role in the THz generation.

Acknowledgment

This work has been partially supported by DGA and CNRS, France.

References

[1] Bass M, Franken P A, Ward J F and Weinreich G 1962 *Phys. Rev. Lett.* **9** 446
Nahata A, Welling A S and Heinz T F 1996 *Appl. Phys. Lett.* **69** 2321
[2] Dai J, Xie X and Zhang X-C 2006 *Phys. Rev. Lett.* **97** 103903
[3] Cook D J and Hochstrasser R M 2000 *Opt. Lett.* **25** 1210
[4] Bartel T, Gaal P, Reimann K, Woerner M and Elsaesser T 2005 *Opt. Lett.* **30** 2805
[5] Cheng C C, Wright E M and Moloney J V 2001 *Phys. Rev. Lett.* **87** 213001
[6] Sprangle P, Peñano J, Hafizi B and Kapetanakos C 2004 *Phys. Rev.* E **69** 066415
[7] Hoyer W, Knorr A, Moloney J V, Wright E M, Kira M and Koch S W 2005 *Phys. Rev. Lett.* **94** 115004
[8] Tzortzakis S *et al* 2002 *Opt. Lett.* **27** 1944
[9] D'Amico C, Houard A, Franco M, Prade B and Mysyrowicz A 2007 *Opt. Express* **15** 15274
[10] Méchain G, D'Amico C, André Y-B, Tzortzakis S, Franco M, Prade B, Mysyrowicz A, Couairon A, Salmon E and Sauerbrey R 2005 *Opt. Commun.* **247** 171
[11] Golubtsov I S, Kandidov V P and Kosareva O G 2003 *Quantum Electron.* **33** 525
[12] D'Amico C, Houard A, Franco M, Prade B, Couairon A, Tikhonchuk V T and Mysyrowicz A 2007 *Phys. Rev. Lett.* **98** 235002
[13] Strickland D and Mourou G 1985 *Opt. Commun.* **56** 219
[14] Braun A, Korn G, Liu X, Du D, Squier J and Mourou G 1995 *Opt. Lett.* **20** 73
[15] Couairon A and Mysyrowicz A 2007 *Phys. Rep.* **441** 47
[16] Tzortzakis S, Franco M, André Y-B, Chiron A, Lamouroux B, Prade B and Mysyrowicz A 1999 *Phys. Rev.* E **60** R3505
[17] Couairon A 2003 *Phys. Rev.* A **68** 015801
[18] Hauri C P, Kornelis W, Helbing F W, Couairon A, Mysyrowicz A, Biegert J and Keller U 2004 *Appl. Phys.* B **79** 673
[19] Couairon A, Biegert J, Hauri C P, Kornelis W, Helbing F W, Keller U and Mysyrowicz A 2006 *J. Mod. Opt.* **53** 75
[20] Chakraborty H S, Gaarde M B and Couairon A 2006 *Opt. Lett.* **31** 3662
[21] Zaïr A, Guandalini A, Schapper F, Holler M, Biegert J, Gallmann L, Keller U, Couairon A, Franco M and Mysyrowicz A 2007 *Opt. Express* **15** 5394
[22] Couairon A, Méchain G, Tzortzakis S, Franco M, Lamouroux B, Prade B and Mysyrowicz A 2003 *Opt. Commun.* **225** 177
[23] Philip J, D'Amico C, Chériaux G, Couairon A, Prade B and Mysyrowicz A 2005 *Phys. Rev. Lett.* **95** 163901
[24] D'Amico C, Prade B, Franco M and Mysyrowicz A 2006 *Appl. Phys.* B **85** 49
[25] Méchain G, Couairon A, Franco M, Prade B and Mysyrowicz A 2004 *Phys. Rev. Lett.* **93** 035003
[26] Musin R R, Shneider M N, Zheltikov A M and Miles R B 2007 *Appl. Opt.* **46** 5593

[27] Kolesik M, Wright E M and Moloney J V 2004 *Phys. Rev. Lett.* **92** 253901
[28] Faccio D, Matijosius A, Dubietis A, Piskarkas R, Varanavicius A, Gaizauskas E, Piskarkas A, Couairon A and Di Trapani P 2005 *Phys. Rev.* E **72** 037601
[29] Couairon A, Gaizauskas E, Faccio D, Dubietis A and Di Trapani P 2006 *Phys. Rev.* E **73** 016608
[30] Faccio D, Averchi A, Couairon A, Dubietis A, Piskarskas R, Matijosius A, Bragheri F, Porras M A, Piskarskas A and Di Trapani P 2006 *Phys. Rev.* E **74** 047603
[31] Faccio D, Porras M A, Dubietis A, Tamosauskas G, Kucinskas E, Couairon A and Di Trapani P 2006 *Opt. Commun.* **265** 672
[32] Faccio D, Porras M A, Dubietis A, Bragheri F, Couairon A and Di Trapani P 2006 *Phys. Rev. Lett.* **96** 193901
[33] Bragheri F, Faccio D, Couairon A, Matijosius A, Tamosauskas G, Varanavicius A, Degiorgio V, Piskarskas A and Di Trapani P 2007 *Phys. Rev.* A **76** 025801
[34] Porras M A, Parola A, Faccio D, Couairon A and Di Trapani P 2007 *Phys. Rev.* A **76** 011803
[35] Zheng J, Yu C X, Zheng Z J and Tanaka K A 2005 *Phys. Plasmas* **12** 093105
[36] Jackson J D 1965 *Classical Electrodynamics* 3rd edn (New York: Wiley)
[37] Houard A, Liu Y, Prade B, Mysyrowicz A and Leriche B 2007 *Appl. Phys. Lett.* **91** 241105
[38] Méchain G *et al* 2003 *Appl. Phys.* B **77** 707
[39] Kasparian J *et al* 2003 *Science* **301** 61
[40] Dubietis A, Couairon A, Kucinskas E, Tamosauskas G, Gaizauskas E, Faccio D and Di Trapani P 2006 *Appl. Phys.* B **84** 439
[41] Cook D J, Chen J X, Morlino E A and Hochstrasser R M 1999 *Chem. Phys. Lett.* **309** 221
[42] Agostini P, Fabre F, Mainfray G and Petit F 1979 *Phys. Rev. Lett.* **42** 1127
[43] Bucksbaum P H, Freeman R R, Bashkansky M and McIlrath T J 1987 *J. Opt. Soc. Am.* **4** 760
[44] McIlrath T J, Bucksbaum P H, Freeman R R and Bashkansky M 1987 *Phys. Rev.* A **35** 4611
[45] Hunter S R, Carter J G and Christophorou G 1988 *Phys. Rev.* A **38** 5539
[46] Frost L S and Phelps A V 1964 *Phys. Rev.* **136** A1538
[47] Freeman R R, Bucksbaum P H, Milchberg H, Darack S, Schumacher D and Geusic M E 1987 *Phys. Rev. Lett.* **59** 1092